online data

Solution structure and backbone dynamics of human epidermal-type fatty acid-binding protein (E-FABP)

Luis H. GUTIÉRREZ-GONZÁLEZ*, Christian LUDWIG*[1], Carsten HOHOFF†[2], Martin RADEMACHER*, Thorsten HANHOFF†, Heinz RÜTERJANS*, Friedrich SPENER† and Christian LÜCKE*[3]

*Institut für Biophysikalische Chemie, Johann Wolfgang Goethe-Universität Frankfurt, Marie-Curie-Strasse 9, D-60439 Frankfurt am Main, Germany, and †Institut für Biochemie, Westfälische Wilhelms-Universität Münster, Wilhelm-Klemm-Strasse 2, D-48149 Münster, Germany

Human epidermal-type fatty acid-binding protein (E-FABP) belongs to a family of intracellular 14–15 kDa lipid-binding proteins, whose functions have been associated with fatty acid signalling, cell growth, regulation and differentiation. As a contribution to understanding the structure–function relationship, we report in the present study features of its solution structure and backbone dynamics determined by NMR spectroscopy. Applying multi-dimensional high-resolution NMR techniques on unlabelled and ^{15}N-enriched recombinant human E-FABP, the ^{1}H and ^{15}N resonance assignments were completed. On the basis of 2008 distance restraints, the three-dimensional solution structure of human E-FABP was subsequently obtained (backbone atom root-mean-square deviation of 0.92 ± 0.11 Å; where 1 Å = 0.1 nm), consisting mainly of 10 anti-parallel β-strands that form a β-barrel structure. ^{15}N relaxation experiments (T_1, T_2 and heteronuclear nuclear Overhauser effects) at 500, 600 and 800 MHz provided information on the internal dynamics of the protein backbone. Nearly all non-terminal backbone amide groups showed order parameters $S^2 > 0.8$, with an average value of 0.88 ± 0.04, suggesting a uniformly low backbone mobility in the nanosecond-to-picosecond time range. Moreover, hydrogen/deuterium exchange experiments indicated a direct correlation between the stability of the hydrogen-bonding network in the β-sheet structure and the conformational exchange in the millisecond-to-microsecond time range. The features of E-FABP backbone dynamics elaborated in the present study differ markedly from those of the phylogenetically closely related heart-type FABP and the more distantly related ileal lipid-binding protein, implying a strong interdependence with the overall protein stability and possibly also with the ligand-binding affinity for members of the lipid-binding protein family.

Key words: fatty acid carrier, lipid-binding protein, NMR spectroscopy, ^{15}N relaxation, psoriasis.

INTRODUCTION

The human epidermal-type fatty acid-binding protein (E-FABP) was originally detected in patients suffering from psoriasis, a hyperproliferative skin disease characterized by abnormal differentiation and disordered lipid metabolism [1]. In this pathological situation, E-FABP was immunohistochemically localized in differentiated keratinocytes [2]. The protein is identical with a melanogenic inhibitor isolated from grafted human skin; it inhibits tyrosinase activity in normal melanocytes as well as in a melanoma cell line and reduces cellular proliferation of these cells when added exogenously, whereas normal skin fibroblasts remain unaffected [3].

FABPs, in general, form a family of small (14–15 kDa) cytosolic non-enzymic proteins that display tissue-specific expression and may play a role in fatty acid signalling [4–6], cell growth and differentiation [7,8]. It has also been proposed that these proteins are involved in the cellular uptake of lipids, their transport to metabolic pathways [9] and in the regulation of metabolizing proteins [10]. All of these proteins have 127–135 amino acids and are phylogenetically related. Sequence similarities among the various FABPs range between 38–70 % [11]. Generally, for sequences of orthologous types isolated from different host organisms, the degree of similarity is high, whereas, for paralogous types of the same host organism, the similarities are generally lower. Numerous members of this protein family have been isolated from a variety of mammalian, avian and fish tissues as well as from insects [12,13].

FABPs belong to a larger family of intracellular lipid-binding proteins (LBPs) that display amino acid motifs aimed at high-affinity binding of amphiphilic ligands, such as long-chain fatty acids, bile acids, retinoids and eicosanoids. Tertiary structures found in this protein family show a highly conserved folding motif, i.e. a β-barrel consisting of two orthogonal β-sheets with five anti-parallel β-strands each and a helix-turn-helix domain partially covering the internal water-filled cavity [14]. The ligand is non-covalently bound inside the cavity, almost inaccessible to the external solvent. LBPs can be grouped according to sequence

Abbreviations used: FABP, fatty acid-binding protein; A-FABP, adipocyte-type FABP; E-FABP, epidermal-type FABP; H-FABP, heart-type FABP; M-FABP, myelin-type FABP; I-FABP, intestinal-type FABP; ILBP, ileal lipid-binding protein; LBP, lipid-binding protein; NOE, nuclear Overhauser effect; HSQC, heteronuclear single-quantum coherence; RMSD, root-mean-square deviation; 2D, two-dimensional; 3D, three-dimensional.

[1] Present address: Department of Immunology and Biochemistry, St. George's Hospital Medical School, Cranmer Terrace, London SW17 0RE, U.K.
[2] Present address: Institut für Rechtsmedizin, Universitätsklinikum Münster, Röntgenstrasse 23, D-48149 Münster, Germany.
[3] To whom correspondence should be addressed (e-mail lueck@bpc.uni-frankfurt.de).

The ^{1}H and ^{15}N resonance assignments for recombinant human E-FABP have been deposited at the BioMagResBank (http://www.bmrb.wisc.edu) under the accession number BMRB-5083. The atom co-ordinates of the 20 conformers representing the solution structure of human E-FABP have been deposited at the Research Collaboratory for Structural Bioinformatics ('RCSB') Protein Data Bank (http://www.rcsb.org) under the accession number 1JJJ.

homology, which is consistent with the ligand-binding characteristics [15]: (*I*) the intracellular retinoid-binding proteins; (*II*) the ileal lipid-binding protein (ILBP), which binds bile acid, and the liver-type FABP ('L-FABP'), which binds two fatty acids; (*III*) intestinal-type FABP (I-FABP), which binds a single fatty acid in a linear conformation; and (*IV*) FABPs with the fatty acid bound in a highly bent or U-shaped conformation. The E-FABP examined in the present study belongs to the last group along with adipocyte-type FABP (A-FABP), brain-type FABP ('B-FABP'), heart-type FABP (H-FABP) and myelin-type FABP (M-FABP), where the carboxylate end of the fatty acid is buried within the binding cavity and forms hydrogen bonds with highly conserved tyrosine and arginine residues, either directly or through an ordered water molecule. The hydrocarbon tail of the fatty acid forms van der Waals interactions with hydrophobic residues in the binding cavity and with ordered water molecules that are in contact with polar residues inside the binding pocket [16].

Recombinant human E-FABP consists of 135 amino acids (15.2 kDa) and shows strong binding to stearic acid. The binding affinity decreases on reduction of the number of carbon atoms in the acyl chain or the introduction of double bonds [2]. Moreover, E-FABP displays a different electrophoretic mobility compared with FABPs from other human tissues or cellular retinoid-binding proteins. Another unique feature of orthologous E-FABPs is the presence of 5–6 conserved cysteine residues, a number unusually high for members of this protein family. The crystallographic structure of human E-FABP, solved recently by Hohoff et al. [17], showed the existence of a single disulphide bridge between Cys^{120} and Cys^{127}, the only reported case in the entire LBP family. Moreover, it is known that E-FABP forms a complex with psoriasin (also known as S100A7) [18], a protein of the S100 gene family that has been associated with psoriasiform epidermal hyperplasia and is secreted by neoplastic keratinocytes in bladder and breast carcinomas [19,20]. Thus an investigation of the E-FABP: psoriasin complex in solution may eventually be useful in understanding the co-ordinated up-regulation of E-FABP and S100A7 in psoriasis.

In addition to the solution structure of human E-FABP complexed with stearic acid, the present study describes the protein backbone dynamics determined by means of ^{15}N relaxation (T_1 and T_2) and steady-state heteronuclear ^{15}N-{^1H} nuclear Overhauser effect (NOE) measurements. Protein dynamics is an important aspect of the relationship between structure and function for most biochemical processes. Previously observed differences in the hydrogen-exchange behaviour of backbone amide protons have indicated that proton stability and dynamics are distinct for several LBPs [21]. Thus ^{15}N backbone relaxation experiments may shed more light on the differences in the dynamics between the various members of this protein family. The backbone relaxation and hydrogen/deuterium exchange data obtained in the present study for human E-FABP in complex with stearic acid are compared with those of other LBPs in order to gain a better understanding of the relationships between their structure, dynamics and function.

EXPERIMENTAL

Protein preparation

Recombinant human E-FABP was heterologously expressed in *Escherichia coli* and purified as described by Hohoff et al. [17]. To obtain ^{15}N-enriched E-FABP, the protein was expressed in M9 minimal medium with $^{15}NH_4Cl$ (Cambridge Isotope Laboratories, Andover, MA, U.S.A.) as the sole nitrogen source. All protein samples were delipidated with Lipidex-1000 as described by Glatz and Veerkamp [22], and subsequently re-lipidated using a 3-fold excess of stearic acid ($C_{18:0}$), for which E-FABP shows the highest binding affinity [2].

Recombinant bovine H-FABP was prepared and delipidated as reported previously [23]. The hydrogen/deuterium exchange of H-FABP in the apo-form (1.2 mM) was performed as described previously for holo H-FABP [24]. A series of homonuclear one-dimensional and two-dimensional (2D) NMR experiments were collected at a temperature of 310 K and a ^1H resonance frequency of 600.13 MHz to follow the amide–proton exchange over time.

NMR data collection and processing

The NMR data collection was performed at pH 5.6 and 298 K. The 3–4 mM E-FABP samples were prepared in 20 mM KH_2PO_4 buffer containing 0.05 % NaN_3 and 10 % (v/v) ^2H_2O.

Homonuclear TOCSY and NOESY as well as ^{15}N-edited heteronuclear triple-quantum coherence ('HTQC'), heteronuclear single-quantum coherence (HSQC), TOCSY-HSQC and NOESY-HSQC experiments were carried out on a Bruker DMX spectrometer (Karlsruhe, Germany) operating at a ^1H resonance frequency of 600.13 MHz and using a 5 mm triple-resonance ($^1H/^{13}C/^{15}N$) probe with XYZ-gradient capability. The TOCSY experiments were performed with spinlock times of either 80 or 4.8 ms (to obtain COSY-type information with less spectral overlap). For the NOESY experiments, mixing times between 150–200 ms were used. The homonuclear TOCSY and NOESY spectra were recorded in a phase-sensitive mode with time-proportional phase incrementation of the initial pulse. Quadrature detection was used in both dimensions with the carrier placed in the centre of the spectrum on the water resonance. The water signal was suppressed by selective presaturation during the relaxation delay. In the NOESY experiments water saturation was also applied during the mixing time. All three-dimensional (3D) experiments made use of pulsed-field gradients for coherence selection and artefact suppression, and utilized gradient-sensitivity-enhancement schemes when appropriate [25,26]. Quadrature detection in the indirectly detected dimensions was achieved using either the States/TPPI (time-proportional phase incrementation) or the echo/anti-echo method. Baseline corrections were applied wherever necessary. All spectra were calibrated with respect to 2,2-dimethyl-2-silapentane-5-sulphonate (Cambridge Isotope Laboratories) as an external reference [27].

The spectral data were processed on a Silicon Graphics workstation using the Bruker XWIN-NMR 1.3 software package. Peak-picking and data analysis of the transformed spectra were performed with the AURELIA 2.5.9 program (Bruker).

Constraint generation and structure calculation

The ^1H and ^{15}N resonance assignments were obtained via the classical NOE-based assignment strategy of Wüthrich [28]. The NOE-derived distance constraints were determined from 2D homonuclear NOESY and 3D ^{15}N-edited NOESY-HSQC spectra. Automated assignments of the NOEs, on the basis of chemical shifts only, were achieved using a MATLAB 5.0 routine. The upper distance limits were set by an internal calibration on the basis of the intensities of sequential and medium-range NOEs from residues located within well-defined secondary structure elements. The cross-peak intensities were grouped into four different distance categories: 2.5, 3.5, 4.5 and 6.0 Å (1 Å = 0.1 nm). Experimental evidence for hydrogen bonds was obtained from hydrogen/deuterium exchange in perdeuterated buffer (20 mM KH_2PO_4 containing 0.05 % NaN_3, pH 7.6, uncorrected reading) after 80 min at 298 K. The structure calculations were

performed with the DYANA 1.5 program package [29], which uses simulated annealing in combination with molecular dynamics in torsion angle space. Assignments of ambiguous NOE cross-peaks were made by applying a structure-aided filtering strategy in repeated rounds of structure calculations. Starting *ab initio*, 300 conformers were calculated in 8000 annealing steps each. A total of 126 stereospecific assignments of prochiral methylene and isopropyl groups were obtained with the program GLOMSA [30]. Pseudo-atom correction for unassigned stereo partners and magnetically equivalent protons was applied as proposed by Wüthrich et al. [31]. Subsequent energy minimization in the presence of the NMR restraints was performed on the 20 best DYANA conformers by using the DISCOVER module of the INSIGHT 97 software package (Molecular Simulations Inc., San Diego, CA, U.S.A.). The consistent valence force field [32] was used with a dielectric constant equal to r (distance in Å). A force constant of 20 kcal·mol^{-1}·Å^{-2} (1 cal ≡ 4.184 J) was used in the NOE restraint term. The resulting structures were analysed with PROCHECK-NMR [33].

Relaxation measurements

T_1, T_2 and steady-state heteronuclear ^{15}N-{^{1}H} NOE measurements were performed according to known pulse schemes with a gradient-selected echo/anti-echo sensitivity enhancement technique [34,35]. For the longitudinal (R_1) and transverse (R_2) relaxation rate constants, a series of 8–12 spectra with relaxation periods between 16–960 ms for T_1 and 25–282 ms for T_2 were collected on Bruker DMX spectrometers operating at ^{1}H resonance frequencies of 499.87, 600.13 and 800.13 MHz. The R_1 and R_2 rates were determined by non-linear least squares fitting of the peak intensities versus mixing time, using mono-exponential functions provided in the RMX software package developed in our laboratory by Jürgen Schmidt (presently at the National Institute for Medical Research, London, U.K.). Steady-state heteronuclear ^{15}N-{^{1}H} NOE values were obtained from the ratio of the peak intensities observed with and without ^{1}H saturation. In order to suppress time- or temperature-dependent effects, the spectra were acquired in an interleaved mode with incremented relaxation delays. All experiments were recorded with 256 t_1 increments of 2048 data points in t_2. The spectral widths were set to 6010 Hz (^{1}H)/1773 Hz (^{15}N) at 500 MHz, 7184 Hz (^{1}H)/2131 Hz (^{15}N) at 600 MHz and 9766 Hz (^{1}H)/2841 Hz (^{15}N) at 800 MHz.

The overall molecular shape of the members of the FABP family is not exactly spherical, but rather resembles an oblate ellipsoid. The ratio of the principal components of the rotational diffusion tensor, obtained from hydrodynamic calculations using the bead method [36], is 1.00:0.92:0.83 for E-FABP. This suggests a small degree of anisotropy for the overall rotation of E-FABP, which can, in principle, be detected by NMR relaxation measurements [37]. Since the anisotropy of the rotational diffusion tensor is rather small, however, anisotropic modelling of the global motion does not result in a statistically significant improvement of the fit. Therefore the dynamics calculations were performed by applying an isotropic model in solution, as previously reported for bovine H-FABP and porcine ILBP [38]. Assuming isotropic motion, an estimate of the overall rotational correlation time τ_c was derived using only residues with T_1(N):T_2(N) ratios that fall within one standard deviation of the mean T_1(N):T_2(N) ratio [39].

The microdynamic parameters of the backbone N–H vectors, the generalized order parameter S^2 and the effective correlation time τ_e, as well as the conformational exchange contribution to the transverse relaxation rate, the exchange parameter R_{ex}, were calculated and fitted with the Modelfree4 program of Palmer and co-workers [40,41]. Three models for the spectral density function were applied to derive backbone dynamics information from the experimentally determined relaxation rates R_1, R_2 and NOE. The first model was based on the single timescale model-free formalism proposed by Lipari and Szabo [42,43], with fitting of both S^2 and τ_e. The second model added an R_{ex} term to the model-free formalism, providing fits to S^2 and R_{ex}. Finally, the extended form of the model-free formalism [44] was used as another model of the spectral density function, fitting the parameters S_s^2, S_f^2 and τ_e. S^2 represents the amplitude of the nanosecond-to-picosecond backbone mobility ($S^2 = 1$ corresponds to a completely restricted orientation of the N–H vector, whereas $S^2 = 0$ indicates unrestricted motion). Non-zero values of the transverse relaxation rate R_{ex} are expected to appear when processes of conformational or chemical exchange occur within the millisecond-to-microsecond time range.

RESULTS

Resonance assignments of human E-FABP

Using a series of homonuclear and heteronuclear NMR experiments, the ^{1}H and ^{15}N resonance assignments were completed for recombinant human E-FABP complexed with stearic acid and are available at the BioMagResBank (http://www.bmrb.wisc.edu) under the accession number BMRB-5083. The proton resonance assignments were mainly derived from 2D homonuclear TOCSY and NOESY spectra. ^{1}H/^{15}N-correlated 3D TOCSY-HSQC and 3D NOESY-HSQC spectra were used to identify the ^{15}N resonances of backbone amides and to verify the obtained proton resonance assignments. Side-chain NH_2 resonances were identified using a 2D ^{1}H/^{15}N-heteronuclear triple-quantum coherence spectrum. The sequential resonance assignments of the backbone amide groups are presented in a 2D ^{1}H/^{15}N-HSQC spectrum (Figure 1).

Resonance assignments of FABPs are often hindered by the occurrence of multiple spin-systems. For bovine H-FABP, such spin-system heterogeneities within the so-called 'portal region' indicated up to four separate conformational states due to a mixture of different fatty acid ligands [45]. The portal region is located between helix αII (see Figure 3, right-hand panel for secondary structure denotation) and the turns connecting β-strands βC and βD as well as βE and βF, apparently representing the only opening in the protein surface through which the fatty acid ligand can enter and exit the internal binding cavity [46]. In the case of human E-FABP, however, just nine out of 22 residues that exhibit spin-system heterogeneities are part of this portal region, which encompasses residues 27–39, 57–62 and 76–82. Two separate proton spin-systems were observed for each of the following amino acid residues: Arg^{12} (βA), Val^{28} (αI–αII turn), Met^{35} and Ala^{37} (both αII), Ala^{39} (αII–βB linker), Ile^{44} and Thr^{46} (both βB), Lys^{55} (βC), Gln^{64} (βD), Gly^{70} and Glu^{71} (both βD–βE turn), Thr^{76} (βE), Ala^{78} and Asp^{79} (both βE–βF turn), Phe^{89} (βF), Thr^{90} (βF–βG turn), Val^{95} (βG), Lys^{110} (βH), Val^{121} (βI) and Glu^{135} (C-terminus). Three different proton spin-systems were observed for Gly^{36} (αII) and Thr^{77} (βE–βF turn). Remarkably, the O$^{\gamma}$H resonance of Thr^{77} shows three distinct signals around 5.84 p.p.m., analogous to the corresponding residue Thr^{74} in bovine H-FABP [45]. Moreover, Gly^{36} in α-helix II belongs to a number of sequentially neighbouring residues (Met^{35}, Gly^{36}, Ala^{37} and Ala^{39}) that display multiple spin-systems also in bovine H-FABP (Val^{32}, Gly^{33}, Asn^{34} and Thr^{36}). The same applies to Ala^{78} and Asp^{79} in the βE–βF turn, which correspond to Ala^{75} and Asp^{76} in H-FABP. In contrast with bovine H-FABP, where all these residues showed multiple spin-

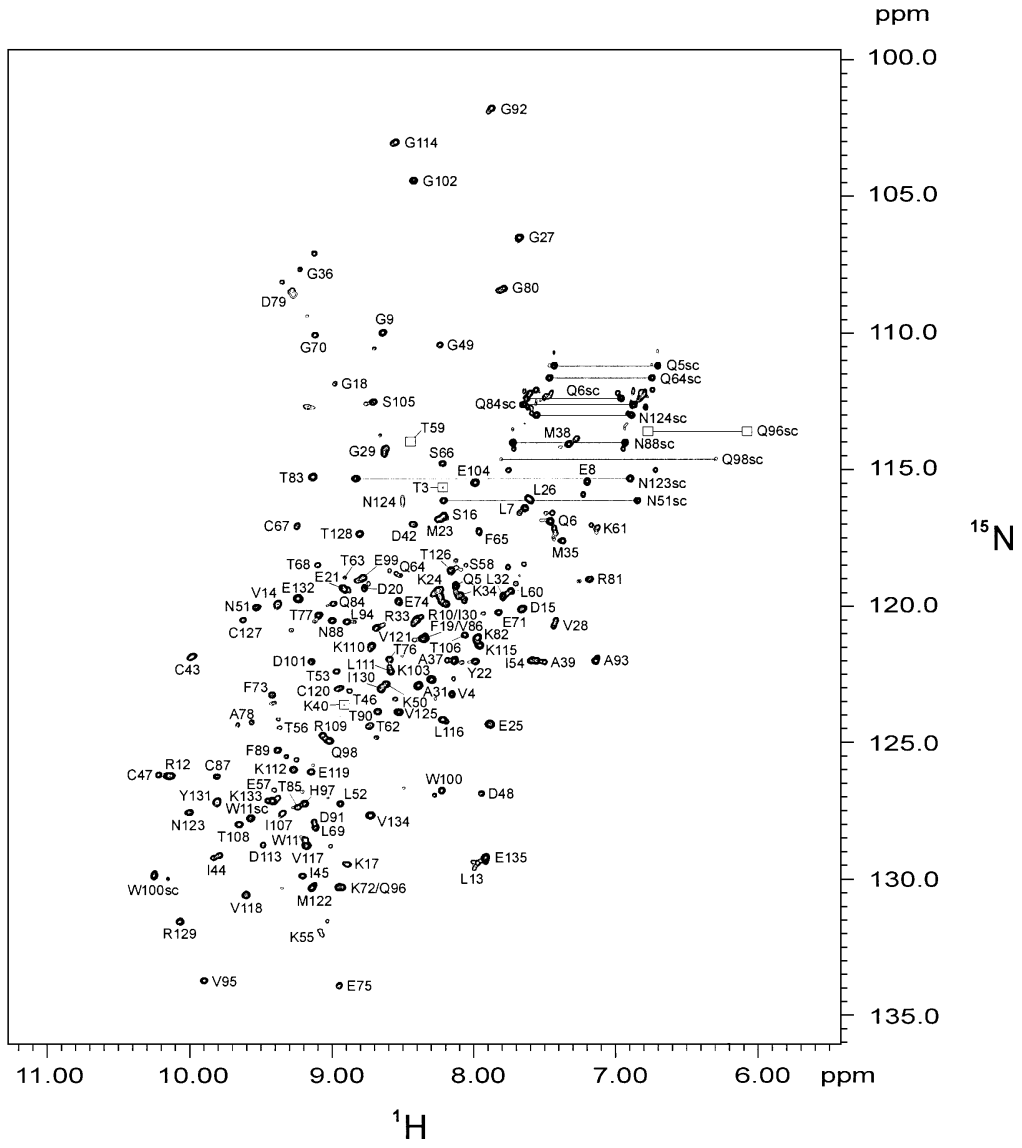

Figure 1 $^{1}H/^{15}N$-HSQC spectrum of human holo E-FABP at pH 5.6 and 298 K (^{1}H resonance frequency of 600.13 MHz)

Backbone and side-chain (sc) amide assignments are shown for each residue. Due to spin-system heterogeneities, several residues display multiple backbone amide signals (not additionally labelled). Peaks observed below the plot level are indicated by squares. Signals from side-chain NH_2 groups are connected by solid lines.

systems of almost the same intensity (representing separate, equally populated conformational states due to different bound fatty acids), one major form is always observed in the spectra of human E-FABP, since the protein had been complexed with only a single type of ligand molecule, i.e. stearic acid. Consequently, the spin-system heterogeneities observed around the portal region in human E-FABP may be due to the presence of a minor ligand-free protein form. All other cases of multiple spin-systems, however, are distributed randomly throughout the amino acid sequence, suggesting a different origin.

The presence of six cysteine residues in the amino acid sequence of human E-FABP is highly unusual for LBPs. Four of the six cysteine residues are unique to the E-FABPs: Cys^{43}, Cys^{47}, Cys^{67} and Cys^{87}. The cysteine residues Cys^{120} and Cys^{127} of E-FABP are partially conserved in some LBPs, but only the M-FABP sequence includes both (at positions 117 and 124 respectively). In the 3D structure of E-FABP, two cysteine residue pairs (Cys^{67}/Cys^{87} and Cys^{120}/Cys^{127}) were identified by X-ray analysis to be close enough to allow disulphide bridge formation, but a disulphide bond was actually found only between Cys^{120} and Cys^{127} [17]. Since the exclusion of a disulphide bridge between Cys^{67} and Cys^{87} improved the R_{free} factor of the crystallographical model, the existence of a covalent bond between these two side chains was considered unlikely. This is in agreement with the NMR data, where $S^{\gamma}H$ resonances have been observed for the cysteine residues Cys^{43}, Cys^{67} (tentative assignment) and Cys^{87}, thus excluding the possibility of a second disulphide bridge in solution.

Solution structure of human E-FABP

To determine the 3D conformation of human E-FABP by NMR spectroscopy, the intensity of the NOE signals obtained from NOESY spectra were translated into pairwise interatomic dis-

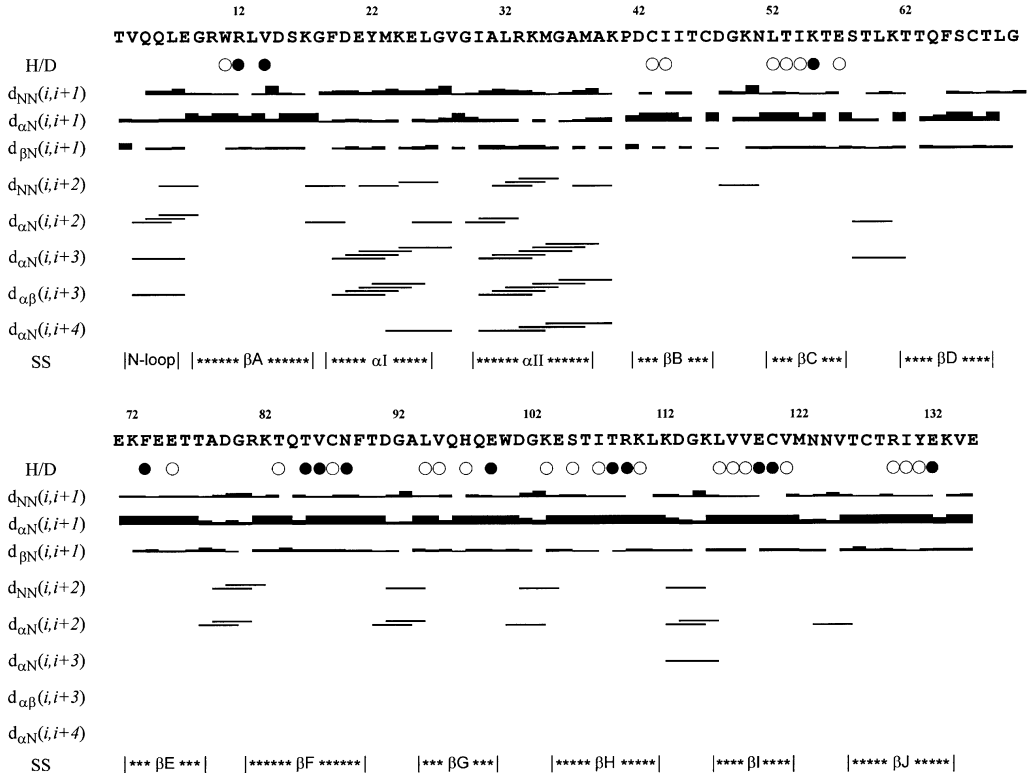

Figure 2 Amino acid sequence of human E-FABP with a survey of the short- and medium-range NOE connectivities, which were used to establish the sequence-specific ^{1}H NMR assignment and to identify elements of regular secondary structure (SS)

H/D indicates residues with slow-exchanging backbone amide protons that remained visible in ^2H_2O solution after 80 min (○) or 2 days (●) at 298 K.

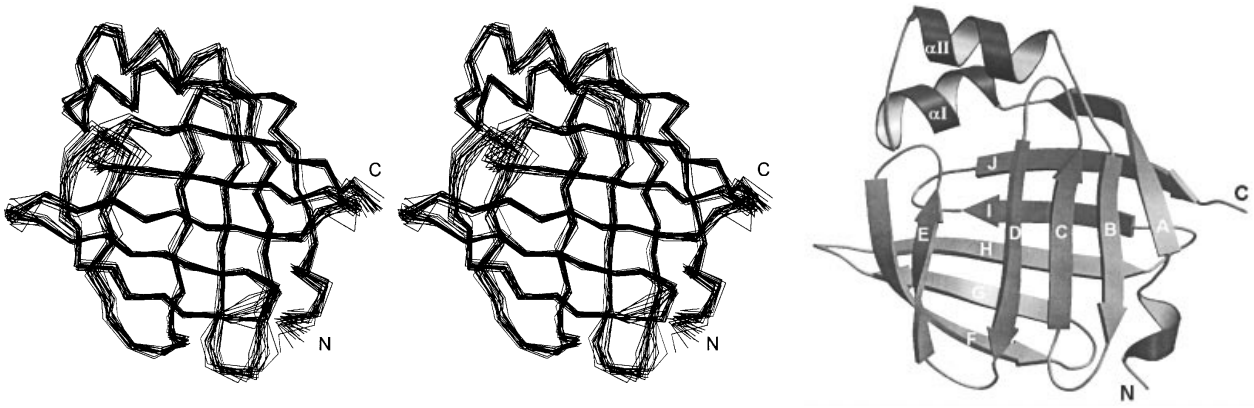

Figure 3 Tertiary structure of human holo E-FABP derived from torsion angle dynamics and restrained energy-minimization calculations

Left-hand and middle panels: stereoview of the ensemble showing the Cα traces of the 20 selected solution structures. Right-hand panel: ribbon drawing showing 10 anti-parallel β-strands (βA–βJ), which are arranged in two almost orthogonal β-sheets forming a β-barrel, and two short α-helices that close the β-barrel structure on one side. The hydrogen-bonding network within the β-sheets is continuous, except for a gap between β-strands βD and βE. The N-terminal residues form an additional helical loop. Produced with MOLSCRIPT [58] and Raster3D [59].

tances. Figure 2 shows the short- and medium-range NOE connectivities assigned to the backbone protons. Helical structures, characterized by strong sequential HN–HN and medium-range HN–HN(i, $i+2$), Hα–HN(i, $i+2$) Hα–HN(i, $i+3$), Hα-Hβ(i, $i+3$) and Hα–HN(i, $i+4$) connectivities, are present in segments Val^4–Leu^7, Phe^{19}–Leu^{26} and Ile^{30}–Met^{38}. NOE connectivity patterns common to anti-parallel β-sheet structures were detected between the backbone protons of β-strands βA–βD and βE–βJ as well as between the N-terminal β-strand βA and the C-terminal β-strand βJ. Backbone amide protons that exchange slowly in ^2H_2O solution due to the hydrogen-bonding network between the β-strands are also indicated in Figure 2. Only between β-strands βD and βE were neither backbone NOE connectivities nor slow-exchanging backbone amide pro-

Table 1 Structural statistics of the 20 selected structures of human E-FABP after energy minimization

Structural statistics	
Total number of residues	133
Total number of distance restraints	2008
Intraresidual	371
Sequential ($\|i–j\| = 1$)	508
Medium-range ($1 < \|i–j\| \leqslant 4$)	233
Long-range ($\|i–j\| > 4$)	896
Hydrogen-bond distance restraints	2×37
Disulphide bridge distance restraints	2×3
Total number of restraint violations > 0.3 Å	0
Total number of restraint violations > 0.2 Å	23
Maximal restraint violation (Å)	0.28
Ramachandran plot statistics (%)	
Residues in most favoured regions	85.1
Residues in additionally allowed regions	13.6
Residues in generously allowed regions	0.6
Residues in disallowed regions	0.7
Structural precision (residues 4–134)	
Backbone atom[a] RMSD (Å)	0.92 ± 0.11
Heavy atom RMSD (Å)	1.46 ± 0.10
Structural precision (residues 4–26, 40–56, 63–75, 83–134)	
Backbone atom[a] RMSD (Å)	0.85 ± 0.10
Heavy atom RMSD (Å)	1.46 ± 0.11

[a] N, C^{α}, C′ and O.

tons observed. This interruption of the β-sheet structure has been referred to as the 'gap' region [14].

On the basis of the NOE and hydrogen-exchange data, an ensemble of 20 energy-minimized conformers representing the solution structure of human E-FABP complexed with stearic acid has been obtained. The analysis of homonuclear 2D NOESY and ^{15}N-edited 3D NOESY spectra led to a total of 2926 NOE-derived distance constraints. Furthermore, 37 slow-exchanging backbone amide protons were identified to be part of the hydrogen-bonding network in the β-sheet and subsequently converted into 74 additional distance constraints. Finally, the disulphide bridge between Cys^{120} and Cys^{127} was defined by three upper and three lower distance bounds. The structure calculation program DYANA regarded 998 of these constraints as irrelevant, i.e. they did not restrict the distance between two protons. Out of the remaining 2008 non-trivial distance constraints, 371 were intraresidual ($i = j$), 508 sequential ($|i–j| = 1$), 233 medium-range ($1 < |i–j| \leqslant 4$), and 896 long-range ($|i–j| > 4$). Figure 3 shows the resulting ensemble of 20 conformers (left-hand and middle panels) as well as the ribbon diagram of the best DYANA structure after restrained energy minimization (right-hand panel). The structure co-ordinates have been deposited at the Research Collaboratory of Scientific Bioinformatics ('RCSB') Protein Data Bank under the accession number 1JJJ. The numbers of experimental distance restraints and other structural statistics of the calculated conformers are listed in Table 1.

The solution structure of human E-FABP consists of 10 anti-parallel β-strands, defining two nearly orthogonal β-sheets of five β-strands each, and two short α-helices that form an helix-turn-helix domain. The centre of β-strand βF (Lys^{82}–Phe^{89}) is shared by both β-sheets. The N-terminal residues Val^{4}–Leu^{7} form a helical loop (presumably 3_{10} conformation), which leads to β-strand βA (Gly^{9}–Lys^{17}). Residues Val^{14} and Asp^{15} create a β-bulge inside β-strand βA. The residue Gly^{18} connects the first β-strand βA with α-helix I, which consists of residues Phe^{19}–Leu^{26}. Residues Gly^{27}–Gly^{29} form a turn that leads into α-helix II, spanning residues Ile^{30}–Met^{38}. The connection between α-helix II and the second β-strand βB (Asp^{42}–Cys^{47}) is made up of residues Ala^{39}–Pro^{41}. The rest of the structure consists of a series of β-strands: βC (Leu^{52}–Glu^{57}), βD (Thr^{62}–Thr^{68}), βE (Lys^{72}–Thr^{77}), βF (Arg^{81}–Phe^{89}), βG (Leu^{94}–Glu^{99}), βH (Glu^{104}–Leu^{111}), βI (Leu^{116}–Val^{121}) and βJ (Thr^{126}–Lys^{133}), which are connected mostly by hairpin turns.

For the 20 best E-FABP conformers, root-mean-square deviation (RMSD) values of 0.92 ± 0.11 Å and 1.46 ± 0.10 Å were determined for the backbone and heavy atoms respectively, excluding the terminal residues. Without the portal region (i.e. for residues 4–26, 40–56, 63–75 and 83–134), a backbone RMSD of 0.85 ± 0.10 Å was obtained, thus reflecting the higher conformational dispersion in the portal region. Superposition with the X-ray structure of human E-FABP (excluding the terminal residues) yielded average backbone RMSD values of 1.00 ± 0.07 Å for the entire residue range and 0.98 ± 0.06 Å without the portal region. This indicates a close similarity between the crystallographical and the solution structures. According to the Ramachandran plot, the backbone dihedral angles of residues within the major secondary structure elements show well-defined values with low standard deviations. A total of 99.3 % of all non-glycine/non-proline residues are found in the allowed regions of conformational space. Most of the cases found in the disallowed regions belong to Val^{4} (N-terminus), Asp^{91} (βF–βG turn) or Asn^{123} (βI–βJ turn), i.e. residues that might not be well-defined in the structure calculation due to rather exposed positions either in turns or at terminal ends.

Backbone dynamics of human E-FABP

In spite of the high degree of structural similarity, most members of the FABP family show marked functional differences. For example, the oleic acid-binding constants vary from 0.44 μM for human H-FABP to 0.82 μM for human E-FABP and $\gg 1$ μM for human ILBP [47]. Since ligand binding may also be influenced by intrinsic dynamical properties of the protein, it is important to characterize the backbone dynamics of E-FABP. ^{15}N longitudinal and transverse relaxation rates as well as heteronuclear NOE values of human holo E-FABP were measured at three different fields (500, 600 and 800 MHz). The experimental values of the relaxation rates R_1 and R_2 are shown in Figure 4. The numerical values of R_1, R_2 and NOE are also listed in the supplemental material (available at http://www.BiochemJ.org/bj/364/bj3640725add.htm), with the error of the NOE set to a constant value (0.03) for all residues. These data were subsequently combined and analysed for 120 of 132 backbone amide groups to yield the microdynamic parameters S^2, τ_e and R_{ex} (Table 2), which provide information about the mobility of the backbone N–H bond vectors, the correlation time of local motion and the conformational exchange contribution to transverse relaxation respectively.

Backbone amide order parameters were determined for all three fields combined, with a resulting molecular tumbling correlation time of $\tau_c = 8.6$ ns. Nearly all non-terminal backbone amide groups showed S^2 values > 0.8, with an average value of 0.88 ± 0.04; the same average S^2 value holds for the residues belonging to the secondary structure elements. As can be seen in Figure 5, S^2 values (representing backbone mobility within the nanosecond-to-picosecond timescale) show little correlation with secondary structure. Interestingly, the N-terminal helical loop and α-helix I both exhibit above-average S^2 values, indicating reduced backbone mobility, whereas α-helix II as part of the portal region displays a higher flexibility. Overall, however, the structure of human E-FABP shows a rather uniform

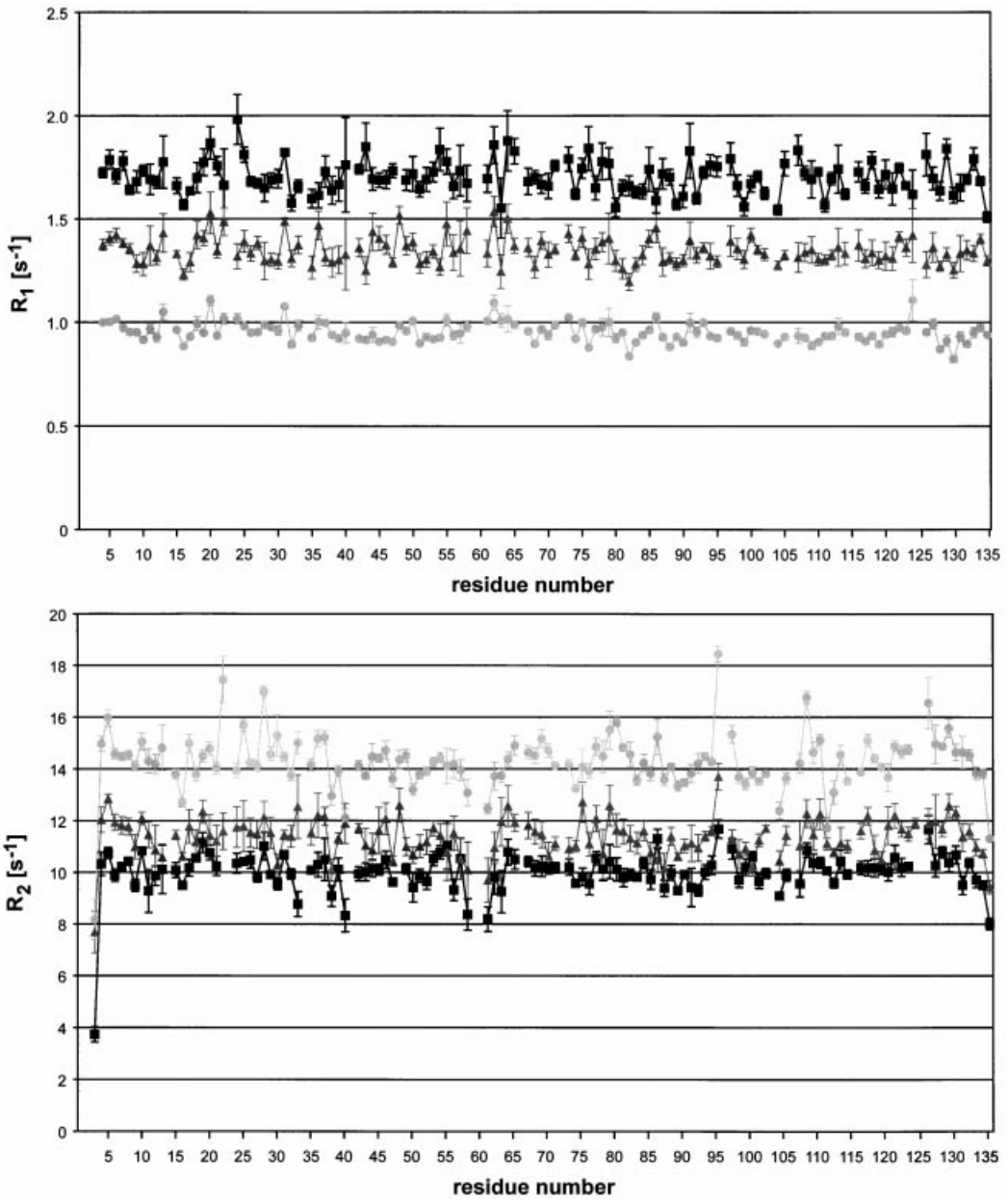

Figure 4 Experimental longitudinal (R_1) and transverse (R_2) relaxation rates

^{15}N relaxation rates obtained for human holo E-FABP at 500 (■), 600 (▲) and 800 (●) MHz. The error bars represent S.D.

dynamic behaviour throughout the entire amino acid sequence. Therefore these data obtained for holo E-FABP suggest a protein backbone structure of relatively low flexibility (S^2 values > 0.8 imply a cone semi-angle of $< 21°$ assuming the wobbling-in-a-cone model for the N–H vector motion).

To better understand the influence of molecular dynamics processes on the functional properties of LBPs, the backbone dynamics data and hydrogen/deuterium exchange behaviour of human E-FABP are compared below with results reported previously for bovine H-FABP and porcine ILBP [38]. Since the ^{15}N relaxation data of both H-FABP and ILBP had been obtained for the apo-forms, we decided to perform an additional hydrogen/deuterium exchange experiment with apo H-FABP for better comparability. Lassen et al. [23] have reported that 70 backbone amide protons displayed very slow exchange in bovine holo H-FABP over a period of several days at 310 K. For the apo-form, we now observed 39 such amide resonances after 4 days under identical conditions. This indicates a lower stability in the hydrogen-bonding network of the β-sheet structure for the apo-form compared with H-FABP complexed with a fatty acid. Such a stabilizing effect due to ligand binding has also been reported previously in the case of porcine ILBP [21]. Still, the amide–proton-exchange behaviour within the β-sheet is also unusually slow for apo H-FABP compared with other LBP types.

Due to the fact that the LBP holo-forms are usually more stable than the apo-forms, as mentioned above, and due to the rather low stability of the E-FABP samples, we have chosen to

Table 2 Microdynamic parameters obtained for human holo E-FABP

Only non-zero values of τ_e and R_{ex} are shown in the table. n.v., residues for which no value could be calculated. The spectral density models are defined, as described in the Experimental section, as: 1, fit of S^2 and τ_e [42,43]; 2, fit of S^2 and R_{ex}; and 3, fit of S_s^2 S_f^2 and τ_e [44]. Error values are S.D.

Amino acid	S^2	τ_e [ps]	R_{ex} [s^{-1}]	Model
Met[1]	n.v.	n.v.	n.v.	
Ala[2]	n.v.	n.v.	n.v.	
Thr[3]	0.382 ± 0.021	5.200 ± 0.793		1
Val[4]	0.925 ± 0.007	5.285 ± 11.370		1
Gln[5]	0.922 ± 0.010		0.746 ± 0.111	2
Gln[6]	0.940 ± 0.007	14.909 ± 13.768		1
Leu[7]	0.925 ± 0.006			1
Glu[8]	0.871 ± 0.006		0.575 ± 0.073	2
Gly[9]	0.897 ± 0.007	2.142 ± 8.065		1
Arg[10]	0.864 ± 0.008		0.748 ± 0.107	2
Trp[11]	0.912 ± 0.015			1
Arg[12]	0.855 ± 0.011		0.511 ± 0.150	2
Leu[13]	0.929 ± 0.056			1
Val[14]	n.v.	n.v.	n.v.	
Asp[15]	0.895 ± 0.005	16.283 ± 7.323		1
Ser[16]	0.827 ± 0.004	6.216 ± 4.010		1
Lys[17]	0.867 ± 0.007	3.133 ± 6.060		1
Gly[18]	0.900 ± 0.008	11.558 ± 8.721		1
Phe[19]	0.934 ± 0.009			1
Asp[20]	0.964 ± 0.016	400.000 ± 607.616		1
Glu[21]	0.904 ± 0.010			1
Tyr[22]	0.953 ± 0.021		0.814 ± 0.318	2
Met[23]	n.v.	n.v.	n.v.	
Lys[24]	0.935 ± 0.012	4.147 ± 13.664		1
Glu[25]	0.911 ± 0.007		0.522 ± 0.089	2
Leu[26]	0.876 ± 0.007		0.544 ± 0.071	2
Gly[27]	0.885 ± 0.007	0.603 ± 7.154		1
Val[28]	0.904 ± 0.014		1.421 ± 0.113	2
Gly[29]	0.884 ± 0.007	27.259 ± 6.935		1
Ile[30]	0.847 ± 0.010	11.991 ± 5.313		1
Ala[31]	0.946 ± 0.005	86.641 ± 18.747		1
Leu[32]	0.858 ± 0.008	14.709 ± 5.730		1
Arg[33]	0.874 ± 0.011	26.347 ± 6.999		1
Lys[34]	n.v.	n.v.	n.v.	
Met[35]	0.873 ± 0.007	10.879 ± 6.427		1
Gly[36]	0.885 ± 0.019		0.793 ± 0.169	2
Ala[37]	0.934 ± 0.007		0.549 ± 0.105	2
Met[38]	0.844 ± 0.010	36.798 ± 5.561		1
Ala[39]	0.861 ± 0.013		0.460 ± 0.109	2
Lys[40]	0.830 ± 0.018	28.825 ± 6.220		1
Pro[41]	n.v.	n.v.	n.v.	
Asp[42]	0.874 ± 0.007		0.456 ± 0.079	2
Cys[43]	0.858 ± 0.013		0.447 ± 0.094	2
Ile[44]	0.885 ± 0.014	10.874 ± 7.513		1
Ile[45]	0.855 ± 0.007		0.691 ± 0.073	2
Thr[46]	0.866 ± 0.010		0.720 ± 0.140	2
Cys[47]	0.845 ± 0.006	10.279 ± 4.851		1
Asp[48]	0.952 ± 0.014			1
Gly[49]	0.905 ± 0.008	0.248 ± 8.901		1
Lys[50]	0.916 ± 0.007	37.914 ± 9.876		1
Asn[51]	0.843 ± 0.007		0.504 ± 0.080	2
Leu[52]	0.857 ± 0.012		0.486 ± 0.098	2
Thr[53]	0.869 ± 0.009		0.573 ± 0.087	2
Ile[54]	0.871 ± 0.009		0.628 ± 0.090	2
Lys[55]	0.933 ± 0.017	14.390 ± 13.568		1
Thr[56]	0.874 ± 0.014			1
Glu[57]	0.911 ± 0.019	32.786 ± 12.775		1
Ser[58]	0.870 ± 0.016	34.945 ± 8.004		1
Thr[59]	n.v.	n.v.	n.v.	
Leu[60]	n.v.	n.v.	n.v.	
Lys[61]	0.875 ± 0.008	52.769 ± 7.593		1
Thr[62]	0.943 ± 0.017	68.162 ± 30.110		1
Thr[63]	0.919 ± 0.014	34.047 ± 12.698		1
Gln[64]	0.976 ± 0.009	215.923 ± 278.933		1
Phe[65]	0.937 ± 0.011			1
Ser[66]	n.v.	n.v.	n.v.	
Cys[67]	0.915 ± 0.008	2.207 ± 9.861		1

Table 2 (contd.)

Amino acid	S^2	τ_e [ps]	R_{ex} [s^{-1}]	Model
Thr[68]	0.847 ± 0.009		0.720 ± 0.120	2
Leu[69]	0.918 ± 0.011			1
Gly[70]	0.903 ± 0.010	4.214 ± 8.854		1
Glu[71]	0.929 ± 0.005			1
Lys[72]	n.v.	n.v.	n.v.	
Phe[73]	0.943 ± 0.008	33.527 ± 15.137		1
Glu[74]	0.874 ± 0.004	3.052 ± 6.068		1
Glu[75]	0.908 ± 0.012	19.284 ± 9.400		1
Thr[76]	0.831 ± 0.009		0.607 ± 0.115	2
Thr[77]	0.918 ± 0.010			1
Ala[78]	0.909 ± 0.018			1
Asp[79]	0.942 ± 0.022	19.671 ± 17.567		1
Gly[80]	0.831 ± 0.013		1.393 ± 0.102	2
Arg[81]	0.875 ± 0.009		0.751 ± 0.076	2
Lys[82]	0.791 ± 0.005		0.863 ± 0.135	2
Thr[83]	0.853 ± 0.005	3.311 ± 5.113		1
Gln[84]	0.884 ± 0.008			1
Thr[85]	0.904 ± 0.010	11.737 ± 8.693		1
Val[86]	0.920 ± 0.013	12.108 ± 10.961		1
Cys[87]	0.878 ± 0.009	4.420 ± 6.704		1
Asn[88]	0.836 ± 0.004		0.701 ± 0.055	2
Phe[89]	0.837 ± 0.005	13.134 ± 4.631		1
Thr[90]	0.840 ± 0.008		0.385 ± 0.072	2
Asp[91]	0.921 ± 0.017	18.261 ± 12.010		1
Gly[92]	0.838 ± 0.009	10.170 ± 4.951		1
Ala[93]	0.931 ± 0.005	22.093 ± 11.121		1
Leu[94]	0.880 ± 0.008		0.525 ± 0.063	2
Val[95]	0.864 ± 0.010		2.160 ± 0.127	2
Gln[96]	n.v.	n.v.	n.v.	
His[97]	0.902 ± 0.009		0.590 ± 0.127	2
Gln[98]	0.883 ± 0.010			1
Glu[99]	0.832 ± 0.012		0.452 ± 0.105	2
Trp[100]	0.902 ± 0.008			1
Asp[101]	0.897 ± 0.005	5.397 ± 7.622		1
Gly[102]	0.864 ± 0.007		0.446 ± 0.066	2
Lys[103]	n.v.	n.v.	n.v.	
Glu[104]	0.817 ± 0.005	22.646 ± 3.745		1
Ser[105]	0.883 ± 0.008			1
Thr[106]	n.v.	n.v.	n.v.	
Ile[107]	0.906 ± 0.015	15.439 ± 9.543		1
Thr[108]	0.867 ± 0.009		1.454 ± 0.104	2
Arg[109]	0.842 ± 0.015		0.785 ± 0.171	2
Lys[110]	0.861 ± 0.007		0.873 ± 0.090	2
Leu[111]	0.844 ± 0.005	33.690 ± 4.649		1
Lys[112]	0.850 ± 0.007	14.900 ± 5.321		1
Asp[113]	0.930 ± 0.016	16.573 ± 13.394		1
Gly[114]	0.844 ± 0.009		0.411 ± 0.071	2
Lys[115]	n.v.	n.v.	n.v.	
Leu[116]	0.869 ± 0.013		0.449 ± 0.084	2
Val[117]	0.847 ± 0.010		0.986 ± 0.101	2
Val[118]	0.882 ± 0.011		0.546 ± 0.092	2
Glu[119]	0.833 ± 0.010		0.690 ± 0.080	2
Cys[120]	0.885 ± 0.011	0.780 ± 7.328		1
Val[121]	0.874 ± 0.017		0.804 ± 0.130	2
Met[122]	0.909 ± 0.006		0.405 ± 0.093	2
Asn[123]	0.849 ± 0.006		0.672 ± 0.075	2
Asn[124]	0.937 ± 0.015	14.704 ± 14.863		1
Val[125]	n.v.	n.v.	n.v.	
Thr[126]	0.896 ± 0.012		0.910 ± 0.268	2
Cys[127]	0.909 ± 0.016			1
Thr[128]	0.824 ± 0.006		1.084 ± 0.060	2
Arg[129]	0.878 ± 0.013		0.939 ± 0.148	2
Ile[130]	0.802 ± 0.011		1.255 ± 0.125	2
Tyr[131]	0.869 ± 0.014			1
Glu[132]	0.848 ± 0.008		0.703 ± 0.092	2
Lys[133]	0.891 ± 0.009	17.646 ± 7.941		1
Val[134]	0.873 ± 0.006	22.218 ± 6.459		1
Glu[135]	0.754 ± 0.007	400.000 ± 50.008		3

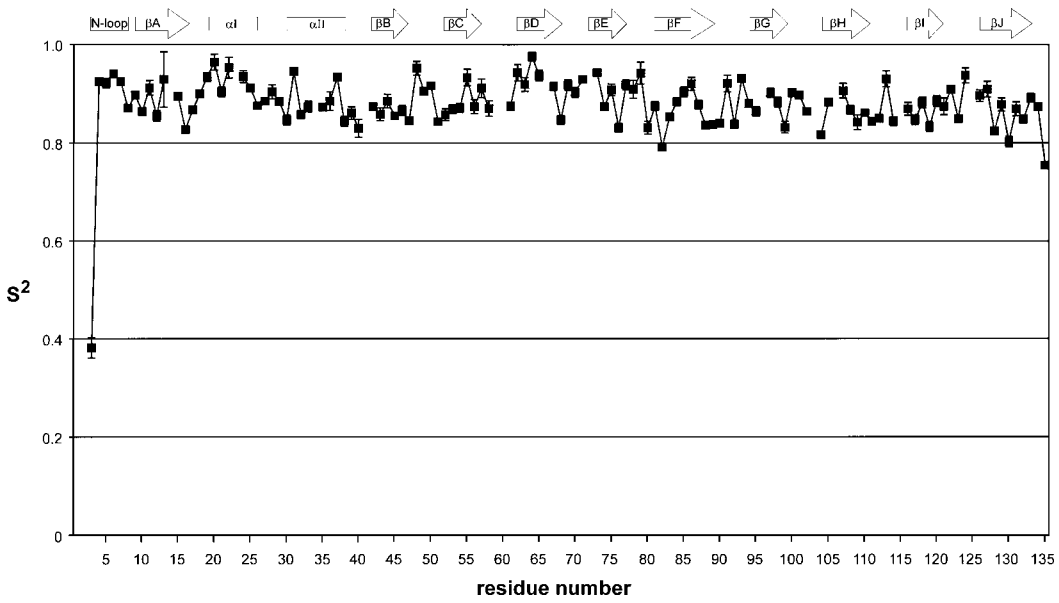

Figure 5 Backbone amide order parameter (S^2) values determined for human holo E-FABP

All non-terminal residues exhibit a rather uniform dynamic behaviour, suggesting a low backbone mobility for the entire protein structure. The secondary structure elements are indicated schematically above the graph. The error bars represent S.D.

investigate human E-FABP in complex with stearic acid at a decreased temperature of 298 K. The comparison with the apo-forms of H-FABP and ILBP [38] should nevertheless provide useful information about the relative conformational stabilities of these FABP types. First, human E-FABP is compared with bovine H-FABP. S^2 distributions of apo H-FABP and holo E-FABP are rather similar, i.e. they show a uniform distribution throughout the amino acid sequence, indicating a relatively low flexibility within the entire backbone structure (average $S^2 = 0.89 \pm 0.06$ for apo H-FABP and 0.88 ± 0.06 for holo E-FABP). However, E-FABP shows a much faster hydrogen exchange compared with H-FABP. For apo H-FABP, 49 slow-exchanging backbone amide protons involved in the hydrogen-bonding network of the β-sheet structure were observed after 6 h in perdeuterated buffer at 310 K (Figure 6A), of which 39 remained detectable after 4 days. On the other hand, in the case of holo E-FABP, only 37 amide proton resonance signals were observable after 2 h in perdeuterated solution at 298 K (Figure 6C), and just 13 signals were still detected after 2 days. Thus compared with apo H-FABP the hydrogen-bonding network in the β-sheet structure of E-FABP is less stable even in the holo-form. Interestingly, in the case of holo E-FABP the analysis of the relaxation data led to R_{ex} values for 47 residues (Figure 6D), the majority of which are located in the centre sections of the β-strands where the slow-exchanging amide protons are also concentrated. This suggests a direct correlation between the slow exchange of backbone amide protons in the β-sheet structure and the occurrence of R_{ex} terms (representing exchange processes on the millisecond-to-microsecond timescale). For apo H-FABP, on the other hand, the occurrence of R_{ex} terms is reduced to only eight residues, which are distributed rather randomly throughout the amino acid sequence (Figure 6B). Since apo H-FABP had been investigated at a considerably higher temperature [23], these results indicate a strongly decreased hydrogen exchange within the β-sheet structure of apo H-FABP relative to holo E-FABP.

Comparing the backbone dynamics data of human E-FABP with the previously reported results for porcine ILBP [38], however, presents a quite different scenario. In the case of apo ILBP, several non-terminal residues displayed strongly decreased S^2 values, suggesting a relatively high flexibility within certain regions of the backbone structure. In addition, an even faster hydrogen exchange was reported for apo ILBP [21] compared with that of holo E-FABP presented in the current study. For apo ILBP, merely 20 amide proton resonance signals remained detectable after only 30 min in perdeuterated solution at 310 K (Figure 6E), all of which disappeared completely after 4 h. ILBP in complex with chenodeoxycholate showed a slower hydrogen exchange relative to apo ILBP, with complete exchange of all backbone amide protons after 18 h at 310 K, thus implying a stabilizing effect induced by the bound ligand. Nevertheless, the exchange of the backbone amide resonances within the β-sheet structure apparently proceeds faster for both apo and holo ILBP than in the cases of apo H-FABP or holo E-FABP, indicating a lower stability of the hydrogen-bonding network in ILBP. Moreover, R_{ex} terms occur in apo ILBP for a total of 43 residues that are located mainly within the β-strands (Figure 6F), suggesting that the exchange of backbone amide protons in this LBP may also be subjected to processes that take place within the millisecond-to-microsecond time range.

DISCUSSION

The solution structure of human E-FABP has been determined by high-resolution NMR spectroscopy on the basis of sequence-specific ^{1}H and ^{15}N resonance assignments. Spin-system heterogeneities were observed for several amino acid residues, in some cases indicating separate backbone conformational states around the portal region. However, even though a weak electron density in the X-ray data of human E-FABP [17] suggested a less well-defined structure in the turn between β-strands βC and βD

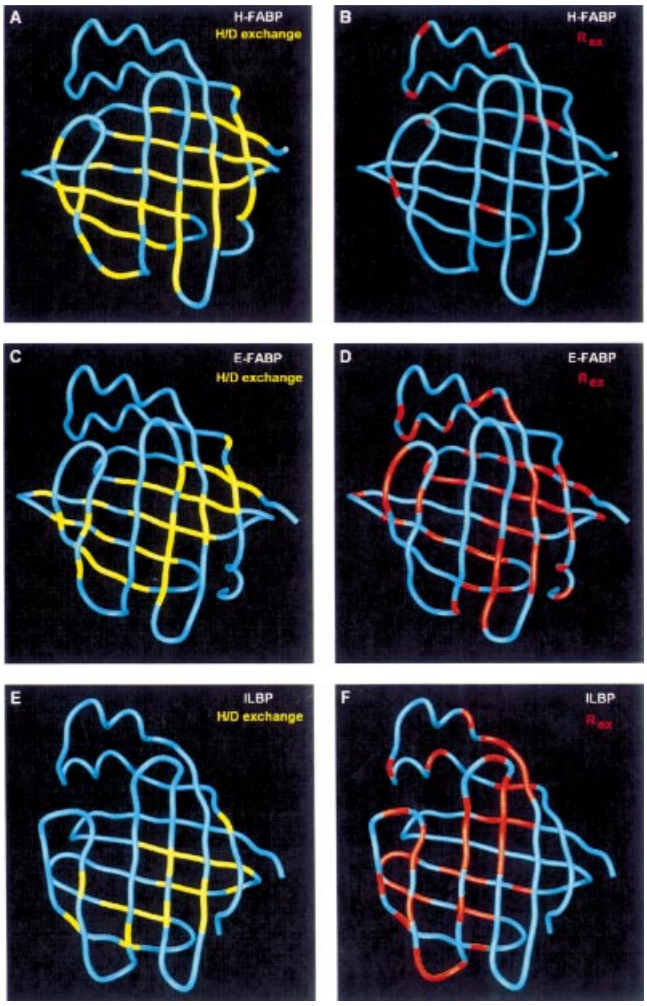

Figure 6 Backbone worm representation indicating slow-exchanging amide protons and non-zero conformational exchange parameter (R_{ex}) values in different LBP family members

Hydrogen/deuterium exchange experiments and the microdynamic parameters obtained from ^{15}N relaxation analysis show significant differences in the chemical exchange with the solvent for the backbone amide protons. In bovine apo H-FABP (**A** and **B**), 49 slow-exchanging amide protons remained visible after 6 h at 310 K in $^{2}H_2O$ solution (**A**), whereas only 8 residues showed exchange parameters (**B**). For human holo E-FABP (**C** and **D**), 37 slow-exchanging amide protons were detected after 2 h at 298 K in $^{2}H_2O$ solution (**C**) and 47 residues with R_{ex} terms occurred in the central β-sheet (**D**). Porcine apo ILBP (**E** and **F**) exhibited 20 slow-exchanging amide protons after 30 min at 310 K in $^{2}H_2O$ solution (**E**) and 43 residues with exchange parameters (**F**). Human holo E-FABP appears to rank between apo H-FABP and apo ILBP in the hydrogen/deuterium exchange, with R_{ex} terms in the β-strands indicating exchange in the millisecond-to-microsecond timescale. Clearly, the hydrogen-bonding network in the β-sheet structure of holo E-FABP is less stable relative to apo H-FABP. R_{ex} values, red; slow-exchanging amide protons (H/D exchange), yellow. Produced using the program GRASP [60].

(comprising residues 58–61 as part of the portal region), no spin-system heterogeneities were observed for these particular residues in the solution structure, thus excluding separate long-lived conformational states as reported for H-FABP [45]. On the other hand, a more 'diffuse' structure in the βC–βD turn, together with a lack of the otherwise highly conserved Phe^{57} ring as a portal lid, might possibly explain the relatively low oleic acid-binding affinity of E-FABP compared with other FABPs in the LBP subfamily *IV* [47].

Furthermore, on the basis of the proton chemical shift assignment, the presence of a second disulphide bridge in human E-FABP can definitely be ruled out. The cystine bond, which has been detected between Cys^{120} and Cys^{127} by the previous X-ray study [17], is unique in the LBP family. Even though biochemical studies have indicated that the respective residues Cys^{117} and Cys^{124} in M-FABP are disulphide linked as well [48], their S^{γ} positions are too far apart (4.5 Å) in the crystal structure for the presence of a disulphide bridge [49]. A comparison with the E-FABP structure provides no obvious explanation for this structural discrepancy observed between these two members of LBP subfamily *IV*, except maybe for the lower atomic resolution (2.7 Å) of the M-FABP data. Still, the high structural homology of this cysteine residue pair strongly suggests the presence of a cystine bond in M-FABP as well, and therefore poses the question why this is not seen in the crystal structure.

The overall structural fold of human E-FABP in solution is very similar to the solution structures of other members of the LBP family, such as H-FABP [23,45], ILBP [21], I-FABP [50,51], as well as cellular retinoic acid-binding protein type II [52] and cellular retinol-binding protein types I and II [53,54]. The presence of an N-terminal helical loop, however, is a unique attribute of the LBP subfamily *IV*. The loop usually consists of four residues, starting with a hydrophobic amino acid, followed by one or two hydrophilic residues and a highly conserved phenylalanine residue (substituted by a leucine residue only in the case of E-FABP) in the last position. The non-polar residues in the first and last position are part of the hydrophobic cluster at the bottom of the protein cavity, whereas the hydrophilic residues are accessible to the external solvent. This additional structural feature in LBP subfamily *IV* might therefore contribute to the overall stability of the β-barrel fold.

Marked differences in conformational stability and binding affinity for fatty acids have been reported for paralogous FABPs of LBP subfamily *IV* [47,55]. In all types of this subgroup, the fatty acid inside the cavity is bound in a U-shaped conformation with hydrogen-bond formation between the carboxylate group and a triad of protein side chains consisting of two arginine residues (one via an ordered water molecule) and one tyrosine residue (E-FABP numbering Arg^{109}, Arg^{129} and Tyr^{131}). Among these FABP types, E-FABP displays the lowest conformational stability in the presence of urea, in spite of the existence of a unique disulphide bridge. Furthermore, E-FABP shows the second lowest binding affinity for oleic acid after A-FABP. In contrast, H-FABP exhibits a very stable conformation and strong ligand binding. A cluster of hydrophobic side chains, which closes the end of the β-barrel structure that is located opposite to the helix-turn-helix domain, might play a significant role in both ligand binding and protein stability. Several members of this hydrophobic cluster are substituted in E-FABP (relative to H-FABP) by residues with different hydrophobicities: Leu^{7} (Phe^{4}), Phe^{65} (Ile^{62}), Cys^{67} (Phe^{64}), Cys^{87} (Val^{84}) and Phe^{89} (Leu^{86}). This might, in part, explain the decreased conformational stability of E-FABP, whereas other substitutions, like Leu^{60} (Phe^{57}) and Val^{118} (Leu^{115}), could be responsible for the weaker binding of fatty acids to E-FABP.

Significant differences in the backbone dynamics between bovine H-FABP and porcine ILBP have been reported previously on the basis of hydrogen/deuterium exchange [21,23] and ^{15}N relaxation experiments [38]. The extremely slow amide–proton-exchange behaviour observed for H-FABP indicated a clear distinction in the stability of the hydrogen-bonding network between these two β-barrel proteins. Hence, both the hydrogen/deuterium exchange behaviour and the microdynamic parameters may provide valuable information about the influence of

molecular dynamic processes on the functional aspects of different LBPs. The backbone dynamics data of human E-FABP were, for this purpose, compared with both bovine H-FABP and porcine ILBP.

The dynamics behaviour of E-FABP contrasts, for example, with that of ILBP [38], which shows a larger spread in the S^2 values and several non-terminal residues, with S^2 values well below 0.7. Yet, other members of the LBP family also exhibit distinct patterns of backbone dynamics. It has been reported, for example, that A-FABP has a greater backbone mobility than H-FABP, especially in the portal region [56]. This is due to the fact that A-FABP has lower S^2 values in the portal region, whereas H-FABP shows higher S^2 values distributed uniformly throughout the amino acid sequence. For I-FABP, on the other hand, a very high mobility around the portal region has been described [57], even though the S^2 values for some residues in this region were abnormally low.

Summarizing the results on protein dynamics obtained in the present study, it can be concluded that the different LBP family members E-FABP, H-FABP and ILBP are characterized by varying stabilities in the protein backbone structures. Hydrogen/deuterium exchange experiments presented significant differences in the chemical exchange with the solvent, for the backbone amide protons belonging to the hydrogen-bonding network in the β-sheets. The β-barrel structure of H-FABP appears to be the most rigid, with exchange processes presumably slower than the millisecond-to-microsecond time range. ILBP, on the other hand, shows the fastest hydrogen exchange as well as a significant number of R_{ex} terms, implying a decreased stability in the β-sheet structure. Finally, E-FABP appears to rank between these two proteins on the basis of the hydrogen/deuterium exchange, with R_{ex} terms in the β-strands indicating millisecond-to-microsecond exchange processes like in ILBP.

According to biochemical data [47], the conformational stabilities of the human paralogues H-FABP, ILBP and E-FABP decrease in this order, which is partially in contrast with the results described in the present study. However, both studies agree that, within LBP subfamily *IV*, the H-FABP has a much more rigid structure than E-FABP. Differences in the arrangement of the hydrophobic cluster inside the protein cavity, in particular the replacement of Phe^4 (H-FABP) by Leu^7 (E-FABP), may be responsible for this distinction. Moreover, the higher conformational stability of H-FABP may also be related to the tighter binding of fatty acid ligands to H-FABP relative to E-FABP [47]. Possibly, there is a correlation between protein stability and ligand-binding affinity, if a more flexible structure allows the bound ligand to leave the binding cavity more easily. On the other hand, the lack of the highly conserved phenylalanine portal lid (Phe^{57} in H-FABP) in E-FABP could be the predominant factor for the lower fatty acid-binding affinities of the latter protein.

Future site-directed mutagenesis studies on human E-FABP may provide definite answers to the questions posed above. Moreover, additional NMR investigations on the dynamics of other intracellular LBPs will be needed for a more concise interpretation of the distinctions in binding affinity and specificity. Finally, the determination of the solution structure of human E-FABP now permits further studies on intermolecular interactions, in particular with S100A7 in regard to psoriasis.

This work was supported in part by the grant SP 135/10-1 from the Deutsche Forschungsgemeinschaft to F.S. We wish to thank David Fushman (University of Maryland) for kindly providing MATLAB routines used in relaxation data analysis. L.H.G.-G. was recipient of a scholarship from the German Academic Exchange Service (DAAD).

REFERENCES

1 Madsen, P., Rasmussen, H. H., Leffers, H., Honoré, B. and Celis, J. E. (1992) Molecular cloning and expression of a novel keratinocyte protein (psoriasis-associated fatty acid binding protein [PA-FABP]) that is highly up-regulated in psoriatic skin and that shares similarity to fatty acid binding proteins. J. Invest. Dermatol. **99**, 299–305
2 Siegenthaler, G., Hotz, R., Chatellard-Gruaz, L., Didierjan, L. and Hellmann, U. (1994) Purification and characterization of the human epidermal fatty acid-binding protein: localization during epidermal cell differentiation *in vivo* and *in vitro*. Biochem. J. **302**, 363–371
3 Farooqui, J. Z., Robb, E., Boyce, S. T., Warden, G. D. and Nordlund, J. J. (1995) Isolation of a unique melanogenic inhibitor from human skin xenografts: initial *in vitro* and *in vivo* characterization. J. Invest. Dermatol. **104**, 739–743
4 Wolfrum, C. and Spener, F. (2000) Fatty acids as regulators of lipid metabolism. Eur. J. Lipid Sci. Technol. **102**, 746–762
5 Wolfrum, C., Borrmann, C. M., Börchers, T. and Spener, F. (2001) Fatty acids and hypolipidemic drugs regulate peroxisome proliferator-activated receptors α- and γ-mediated gene expression via liver fatty acid binding protein: a signaling path to the nucleus. Proc. Natl. Acad. Sci. U.S.A. **98**, 2323–2328
6 Helledie, T., Antonius, M., Sørensen, R. V., Hertzel, A. V., Bernlohr, D. A., Kølvraa, S., Kristiansen, K. and Mandrup, S. (2000) Lipid-binding proteins modulate ligand-dependent *trans*-activation by peroxisome proliferator-activated receptors and localize to the nucleus as well as the cytoplasm. J. Lipid Res. **41**, 1740–1751
7 Yang, Y., Spitzer, E., Kenney, N., Zschiesche, W., Li, M., Kromminga, A., Müller, T., Spener, F., Lezius, A., Veerkamp, J. H. and Smith, G. H. (1994) Members of the fatty acid binding protein family are differentiation factors for the mammary gland. J. Cell Biol. **127**, 1097–1109
8 Delva, L., Bastie, J. N., Rochette-Egly, C., Kraiba, R., Balitrand, N., Despouy, G., Chambon, P. and Chomienne, C. (1999) Physical and functional interactions between cellular retinoic acid binding protein II and the retinoic acid-dependent nuclear complex. Mol. Cell. Biol. **19**, 7158–7167
9 Kaikaus, R. M., Bass, N. M. and Ockner, R. K. (1990) Functions of fatty acid binding proteins. Experientia **46**, 617–630
10 Wolfrum, C., Ellinghaus, P., Fobker, M., Seedorf, U., Assmann, G., Börchers, T. and Spener, F. (1999) Phytanic acid is ligand and transcriptional activator of murine liver fatty acid binding protein. J. Lipid Res. **40**, 704–714
11 Veerkamp, J. H. and Maatman, R. G. (1995) Cytoplasmic fatty acid-binding proteins: their structure and genes. Prog. Lipid Res. **34**, 17–52
12 Bass, N. M. (1988) The cellular fatty acid binding proteins: aspects of structure, regulation, and function. Int. Rev. Cytol. **111**, 143–184
13 Börchers, T. and Spener, F. (1994) Fatty acid binding proteins. Curr. Top. Membr. **40**, 261–294
14 Sacchettini, J. C., Gordon, J. I. and Banaszak, L. J. (1989) Crystal structure of rat intestinal fatty-acid-binding protein. Refinement and analysis of the *Escherichia coli*-derived protein with bound palmitate. J. Mol. Biol. **208**, 327–339
15 Hohoff, C. and Spener, F. (1998) Fatty acid binding proteins and mammary-derived growth inhibitor. Fett/Lipid **100**, 252–263
16 Scapin, G., Young, A. C., Kromminga, A., Veerkamp, J. H., Gordon, J. I. and Sacchettini, J. C. (1993) High resolution X-ray studies of mammalian intestinal and muscle fatty acid-binding proteins provide an opportunity for defining the chemical nature of fatty acid: protein interactions. Mol. Cell. Biochem. **123**, 3–13
17 Hohoff, C., Börchers, T., Rüstow, B., Spener, F. and van Tilbeurgh, H. (1999) Expression, purification, and crystal structure of recombinant human epidermal-type fatty acid binding protein. Biochemistry **38**, 12229–12239
18 Hagens, G., Masouyé, I., Augsburger, E., Hotz, R., Saurat, J.-H. and Siegenthaler, G. (1999) Calcium-binding protein S100A7 and epidermal-type fatty acid-binding protein are associated in the cytosol of human keratinocytes. Biochem. J. **339**, 419–427
19 Celis, J. E., Rasmussen, H. H., Vorum, H., Madsen, P., Wolf, B., Wolf, H. and Orntoft, T. F. (1996) Bladder squamous cell carcinomas express psoriasin and externalize it to the urine. J. Urol. (Baltimore) **155**, 2105–2112
20 Watson, P. H., Leygue, E. R. and Murphy, L. C. (1998) Psoriasin (S100A7). Int. J. Biochem. Cell Biol. **30**, 567–571
21 Lücke, C., Zhang, F., Rüterjans, H., Hamilton, J. A. and Sacchettini, J. C. (1996) Flexibility is a likely determinant of binding in the case of ileal lipid binding protein. Structure (London) **4**, 785–800
22 Glatz, J. F. and Veerkamp, J. H. (1983) Removal of fatty acids from serum albumin by Lipidex 1000 chromatography. J. Biochem. Biophys. Methods **8**, 57–61
23 Lassen, D., Lücke, C., Kveder, M., Mesgarzadeh, A., Schmidt, J. M., Specht, B., Lezius, A., Spener, F. and Rüterjans, H. (1995) Three-dimensional structure of bovine heart fatty-acid-binding protein with bound palmitic acid, determined by multidimensional NMR spectroscopy. Eur. J. Biochem. **230**, 266–280
24 Lücke, C., Lassen, D., Kreienkamp, H.-J., Spener, F. and Rüterjans, H. (1992) Sequence-specific ^{1}H-NMR assignment and determination of the secondary structure of bovine heart fatty-acid-binding protein. Eur. J. Biochem. **210**, 901–910

25 Kay, L. E., Keifer, P. and Saarinen, T. (1992) Pure absorption gradient enhanced heteronuclear single quantum correlation spectroscopy with improved sensitivity. J. Am. Chem. Soc. **114**, 10663–10665

26 Schleucher, J., Sattler, M. and Griesinger, C. (1993) Coherence selection by gradients without signal attenuation: application to the three-dimensional-HNCO experiment. Angew. Chem. Int. Ed. Engl. **32**, 1489–1491

27 Wishart, D. S., Bigam, C. G., Yao, J., Abildgaard, F., Dyson, H. J., Oldfield, E., Markley, J. L. and Sykes, B. D. (1995) ^{1}H, ^{13}C and ^{15}N chemical shift referencing in biomolecular NMR. J. Biomol. NMR **6**, 135–140

28 Wüthrich, K. (1986) NMR of Proteins and Nucleic Acids, John Wiley & Sons, New York

29 Güntert, P., Mumenthaler, C. and Wüthrich, K. (1997) Torsion angle dynamics for NMR structure calculation with the new program DYANA. J. Mol. Biol. **273**, 283–298

30 Güntert, P., Braun, W. and Wüthrich, K. (1991) Efficient computation of three-dimensional protein stuctures in solution from nuclear magnetic resonance data using the program DIANA and the supporting programs CALIBA, HABAS and GLOMSA. J. Mol. Biol. **217**, 517–530

31 Wüthrich, K., Billeter, M. and Braun, W. (1983) Pseudo structures for the 20 common amino acids for use in studies of protein conformations by measurements of intramolecular proton–proton distance constraints with nuclear magnetic resonance. J. Mol. Biol. **169**, 949–961

32 Dauber-Osguthorpe, P., Roberts, V. A., Osguthorpe, D. J., Wolff, D. J., Genest, M. and Hagler, A. T. (1988) Structure and energetics of ligand binding to proteins: *E. coli* dihydrofolate reductase-trimethoprim, a drug receptor system. Proteins: Struct. Funct. Genet. **4**, 31–47

33 Laskowski, R. A., MacArthur, M. W., Moss, D. S. and Thornton, J. M. (1993) AQUA and PROCHECK-NMR: programs for checking the quality of protein structures solved by NMR. J. Appl. Crystallogr. **26**, 283–291

34 Stone, M. J., Fairbrother, W. J., Palmer, A. G., Reizer, J., Saier, Jr, M. H. and Wright, P. E. (1992) The backbone dynamics of the *Bacillus subtilis* glucose permease IIA domain determined from ^{15}N NMR relaxation measurements. Biochemistry **31**, 4394–4406

35 Akke, M., Carr, P. A. and Palmer, A. G. (1994) Heteronuclear correlation NMR spectroscopy with simultaneous isotope filtration, quadrature detection, and sensitivity enhancement using z rotations. J. Magn. Reson. Ser. B **104**, 298–302

36 García de la Torre, J. and Bloomfield, V. (1981) Hydrodynamic properties of complex, rigid, biological macromolecules: theory and applications. Q. Rev. Biophys. **14**, 81–139

37 Tjandra, N., Feler, S. E., Pastor, R. W. and Bax, A. (1995) Rotational diffusion anisotropy of human ubiquitin from ^{15}N NMR relaxation. J. Am. Chem. Soc. **117**, 12562–12566

38 Lücke, C., Fushman, D., Ludwig, C., Hamilton, J. A., Sacchettini, J. C. and Rüterjans, H. (1999) A comparative study of the backbone dynamics of two closely related lipid binding proteins: bovine heart fatty acid binding protein and porcine ileal lipid binding protein. Mol. Cell. Biochem. **192**, 109–121

39 Kay, L. E., Torchia, D. A. and Bax, A. (1989) Backbone dynamics of proteins as studied by ^{15}N inverse detected heteronuclear NMR spectroscopy: application to staphylococcal nuclease. Biochemistry **28**, 8972–8979

40 Mandel, A. M., Akke, M. and Palmer, A. G. (1995) Backbone dynamics of *Escherichia coli* ribonuclease HI: correlations with structure and function in an active enzyme. J. Mol. Biol. **246**, 144–163

41 Palmer, A. G., Rance, M. and Wright, P. E. (1991) Intramolecular motions of a zinc finger DNA-binding domain from Xfin characterized by proton-detected natural abundance ^{13}C heteronuclear NMR spectroscopy. J. Am. Chem. Soc. **113**, 4371–4380

42 Lipari, G. and Szabo, A. (1982) Model-free approach to the interpretation of nuclear magnetic resonance relaxation in macromolecules. 1. Theory and range of validity. J. Am. Chem. Soc. **104**, 4546–4559

43 Lipari, G. and Szabo, A. (1982) Model-free approach to the interpretation of nuclear magnetic resonance relaxation in macromolecules. 2. Analysis of experimental results. J. Am. Chem. Soc. **104**, 4559–4570

44 Clore, G. M., Szabo, A., Bax, A., Kay, L. E., Driscoll, P. C. and Gronenborn, A. M. (1990) Deviations from the two-parameter model-free approach to the interpretation of nitrogen-15 nuclear magnetic relaxation of proteins. J. Am. Chem. Soc. **112**, 4989–4991

45 Lücke, C., Rademacher, M., Zimmerman, A. W., van Moerkerk, H. T. B., Veerkamp, J. H. and Rüterjans, H. (2001) Spin-system heterogeneities indicate a selected-fit mechanism in fatty acid binding to heart-type fatty acid-binding protein (H-FABP). Biochem. J. **354**, 259–266

46 Sacchettini, J. C., Scapin, G., Gopaul, D. and Gordon, J. I. (1992) Refinement of the structure of *Escherichia coli*-derived rat intestinal fatty acid binding protein with bound oleate to 1.75-Å resolution. J. Biol. Chem. **267**, 23534–23545

47 Zimmerman, A. W., van Moerkerk, H. T. B. and Veerkamp, J. H. (2001) Ligand specificity and conformational stability of human fatty acid-binding proteins. Int. J. Biochem. Cell Biol. **33**, 865–876

48 Kitamura, K., Suzuki, M., Suzuki, A. and Uyemura, K. (1980) The complete amino acid sequence of the P2 protein in bovine peripheral nerve myelin. FEBS Lett. **115**, 27–30

49 Cowan, S. W., Newcomer, M. E. and Jones, T. A. (1993) Crystallographic studies on a family of cellular lipophilic transport proteins. Refinement of P2 myelin protein and the structure determination and refinement of cellular retinol-binding protein in complex with *all-trans*-retinol. J. Mol. Biol. **230**, 1225–1246

50 Hodsdon, M. E., Ponder, J. W. and Cistola, D. P. (1996) The NMR solution structure of intestinal fatty acid-binding protein complexed with palmitate: application of a novel distance geometry algorithm. J. Mol. Biol. **264**, 585–602

51 Zhang, F., Lücke, C., Baier, L. J., Sacchettini, J. C. and Hamilton, J. A. (1997) Solution structure of human intestinal fatty acid binding protein: implications for ligand entry and exit. J. Biomol. NMR **9**, 213–228

52 Wang, L., Li, Y., Abildgaard, F., Markley, J. L. and Yan, H. (1998) NMR solution structure of type II human cellular retinoic acid binding protein: implications for ligand binding. Biochemistry **37**, 12727–12736

53 Franzoni, L., Lücke, C., Pérez, C., Cavazzini, D., Rademacher, M., Ludwig, C., Spisni, A., Rossi, G. L. and Rüterjans, H. (2002) Structure and backbone dynamics of apo- and holo-cellular retinol-binding protein in solution. J. Biol. Chem. 10.1074/jbc.M201994200

54 Lu, J., Lin, C.-L., Tang, C., Ponder, J. W., Kao, J. L. F., Cistola, D. P. and Li, E. (2000) Binding of retinol induces changes in rat cellular retinol-binding protein II conformation and backbone dynamics. J. Mol. Biol. **300**, 619–632

55 Veerkamp, J. H. and Zimmerman, A. W. (2001) Fatty acid-binding proteins of nervous tissue. J. Mol. Neurosci. **16**, 133–142

56 Constantine, K. L., Friedrichs, M. S., Wittekind, M., Jamil, H., Chu, C. H., Parker, R. A., Goldfarb, V., Mueller, L. and Farmer, II, B. T. (1998) Backbone and side chain dynamics of uncomplexed human adipocyte and muscle fatty acid-binding proteins. Biochemistry **37**, 7965–7980

57 Hodsdon, M. E. and Cistola, D. P. (1997) Ligand binding alters the backbone mobility of intestinal fatty acid-binding protein as monitored by ^{15}N NMR relaxation and ^{1}H exchange. Biochemistry **36**, 2278–2290

58 Kraulis, P. J. (1991) MOLSCRIPT: a program to produce both detailed and schematic plots of protein structures. J. Appl. Crystallogr. **24**, 946–950

59 Merrit, E. A. and Bacon, D. J. (1997) Raster3D: photorealistic molecular graphics. Methods Enzymol. **277**, 505–524

60 Nicholls, A., Sharp, K. A. and Honig, B. (1991) Protein folding and association: insights from the interfacial and thermodynamic properties of hydrocarbons. Proteins: Struct. Funct. Genet. **11**, 281–296

Received 7 January 2002; accepted 2 April 2002